

MIT Open Access Articles

Real-time, in situ probing of gamma radiation damage with packaged integrated photonic chips

The MIT Faculty has made this article openly available. **Please share** how this access benefits you. Your story matters.

Citation: Du, Qingyang et al. "Real-time, in situ probing of gamma radiation damage with packaged integrated photonic chips." *Photonics Research* 8, 2 (January 2020): 186-193 © 2020 Chinese Laser Press

As Published: <http://dx.doi.org/10.1364/prj.379019>

Publisher: Optical Society of America (OSA)

Persistent URL: <https://hdl.handle.net/1721.1/128110>

Version: Author's final manuscript: final author's manuscript post peer review, without publisher's formatting or copy editing

Terms of use: Creative Commons Attribution-Noncommercial-Share Alike



Real-time, *in-situ* probing of Gamma radiation damage with packaged integrated photonic chips

Qingyang Du¹, Jerome Michon¹, Bingzhao Li², Derek Kita¹, Danhao Ma¹, Haijie Zuo¹, Shaoliang Yu¹, Tian Gu¹, Anuradha Agarwal¹, Mo Li², and Juejun Hu^{1,*}

¹*Department of Materials Science & Engineering, Massachusetts Institute of Technology, Cambridge, Massachusetts, USA*

²*Department of Electrical and Computer Engineering, University of Washington, Seattle, Washington, USA*

*hujuejun@mit.edu

Abstract

Integrated photonics is poised to become a mainstream solution for high-speed data communications and sensing in harsh radiation environments such as outer space, high-energy physics (HEP) facilities, nuclear power plants, and test fusion reactors. Understanding the impact of radiation damage in optical materials and devices is thus a prerequisite to building radiation-hard photonic systems for these applications. In this paper, we report real-time, *in-situ* analysis of radiation damage in integrated photonic devices. The devices, integrated with an optical fiber array package and a baseline-correction temperature sensor, can be remotely interrogated while exposed to ionizing radiations over a long period without compromising their structural and optical integrity. We also introduce a method to deconvolve the radiation damage responses from different constituent materials in a device. The approach was implemented to quantify Gamma radiation damage and post-radiation relaxation behavior of SiO₂-cladded SiC photonic devices. Our findings suggest that densification induced by Compton scattering displacement defects is the primary mechanism for the observed refractive index change in SiC. Additionally, post-radiation relaxation in amorphous SiC does not restore the original pre-irradiated structural state of the material. Our results further point to the potential of realizing radiation-hard photonic device designs taking advantage of the opposite signs of radiation-induced refractive index changes in SiC and SiO₂.

Over the past decade, integrated photonics has rapidly gained recognition as the technology of choice over their electronic counterparts for applications covering data communications¹, radio-frequency (RF) photonics², and on-chip spectroscopic sensing³. Device for operating in harsh radiation environments is yet another arena where integrated photonics presents unique benefits. Integrated photonic modules are being deployed in these settings for applications including optical links for high-volume HEP data transmission⁴ and satellite communications⁵. In addition to their inherent advantages in energy-efficient data communications and non-contact sensing/imaging, recent studies have revealed that various radiation-hard integrated photonic components can be realized with proper designs⁶⁻⁹.

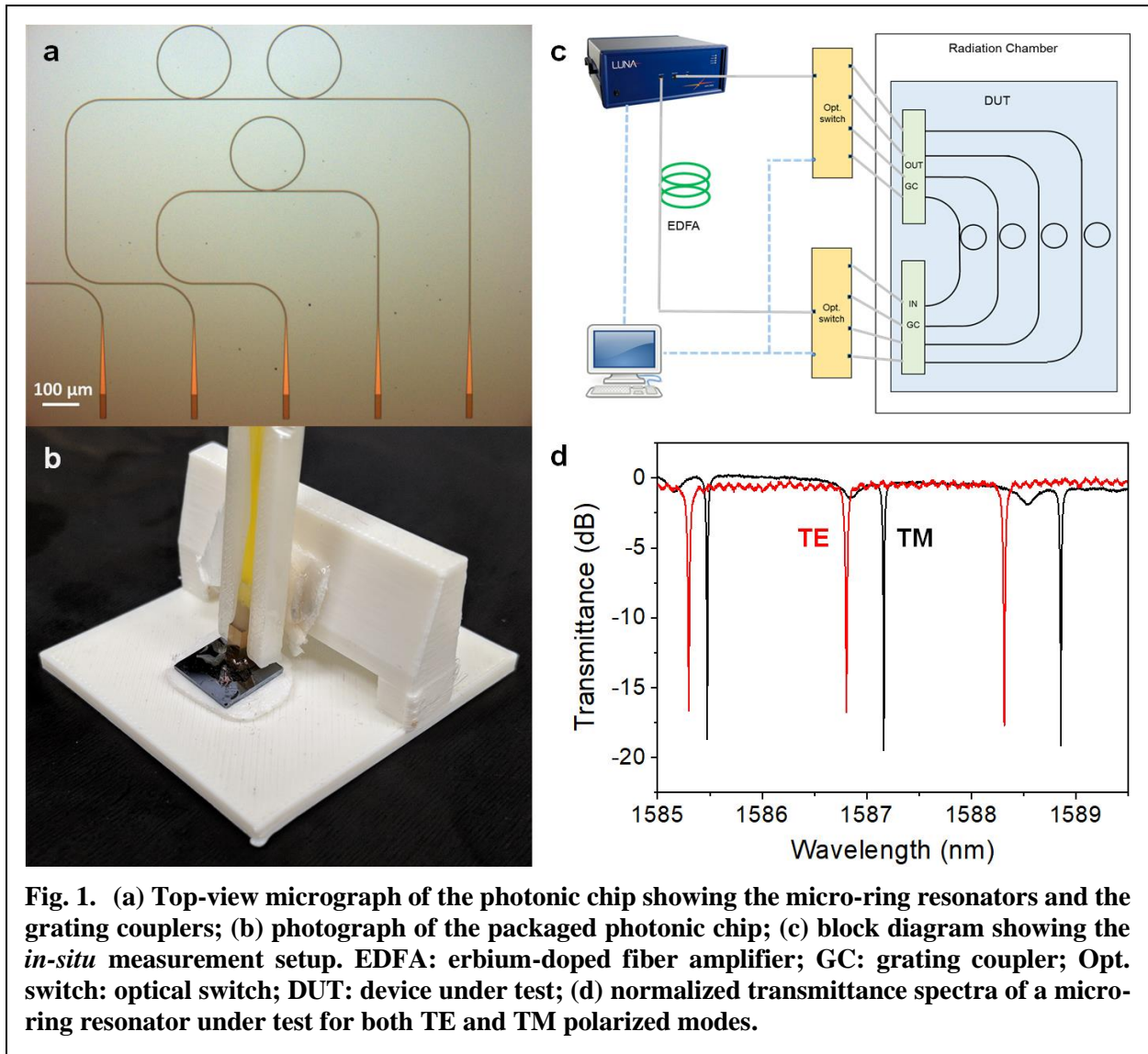
To enable such radiation-hard designs, it is essential to develop thorough understandings about the radiation-induced changes in relevant photonic materials and devices. Towards this goal, several studies have been undertaken to evaluate radiation effects in integrated photonic devices¹⁰⁻¹⁴. In these studies, responses of the photonic devices to ionizing radiations were only quantified *ex-situ*, i.e. after the devices were removed from the irradiation chamber. *In-situ* monitoring of radiation damage has been reported in silicon-on-insulator (SOI) micro-ring resonators (under Gamma ray irradiation)¹⁵ and Mach-Zehnder interferometers (MZIs, under X-ray and neutron irradiation)^{16,17}. The measurements allow for real-time monitoring of the kinetics of radiation damage as well as post-radiation relaxation, which takes place at room temperature and commences immediately after irradiation completes¹⁸.

A standing challenge, however, is that only radiation-induced changes of the overall device response were reported in these studies, and it is unclear which constituent materials are responsible for the performance variation and to what extent. For instance, in an optical waveguide both the core and cladding materials influence its waveguiding properties, and elucidating their relative contributions can open up useful engineering spaces including radiation-hard designs, as we shall discuss later. It is therefore imperative to identify a technique to deconvolve the radiation-induced responses of individual constituent materials.

In this study, we seek to address the challenge by performing real-time measurements of photonic device arrays while they were being irradiated *in-situ*. Stable long-term measurements were made possible by packaging the photonic devices with optical fiber arrays (FAs) as a robust optical interface for light in/out coupling. We further leverage the FAs to facilitate parallel characterization of multiple optical waveguide devices on the same chip. The devices, each designed with a different geometric dimension, gives rise to distinctive optical field distributions in the core and cladding materials. The difference in their radiation-induced responses was then used to isolate the property changes of the core and cladding materials respectively.

Specifically, we employ SiC/SiO₂ as the model system to demonstrate our approach. SiC, which consists of a robust 3-D covalent atomic network interconnected through strong Si-C bonds, has long been regarded as a leading material candidate for radiation-hard devices¹⁹. Recently there is also a surge of interest in SiC for integrated photonics applications covering nonlinear optics, optomechanics, and quantum optics²¹⁻³⁴. In our study, we choose amorphous SiC (a-SiC) deposited using plasma enhanced chemical vapor deposition (PECVD) as the material platform. The choice of PECVD SiC as the waveguide core material is mainly justified by its CMOS compatibility and ease of processing^{20,21}, as neither wafer bonding (in the case of SiC-on-insulator)²²⁻²⁴ nor undercut etch for suspended structures (in the case of epitaxial SiC-on-Si)²⁵⁻³³ is needed. The material processing and device fabrication protocols are detailed in the Methods section. A fiber array consisting of eight optical fiber channels were aligned to the on-chip grating couplers and subsequently permanently attached to the chip using UV-curable epoxy. A thermal couple is also

bonded onto the chip for *in-situ* temperature monitoring. Figure 1b shows a photo of the packaged photonic chip. Prior to irradiation, the temperature-dependent wavelength shifts (TDWS) of the SiC resonator devices under test were quantified and the information was used to correct the resonance drift due to ambient temperature fluctuations during the experiment. The fiber-tethered devices were then loaded into a GammaCell Co-60 Irradiator and exposed to a Gamma ray dose rate of approximately 4,000 rad/min (calibrated with respect to Si). Transmittance spectra of both transverse electric (TE) and transverse magnetic (TM) polarizations were recorded concurrently using an optical vector analyzer (LUNA Technologies OVA-5000) with a built-in external cavity tunable laser. Figure 1c depicts a block diagram illustrating the testing setup and a representative set of measured TE/TM spectra was shown in Fig. 1d.



Long-term stability of the fiber package under Gamma irradiation was experimentally confirmed by examining the loop-back insertion loss variation in the *in-situ* experiment. As is shown in Fig. 2a, changes of the insertion losses remain negligible up to a large irradiation dose of 10 Mrad and are consistently less than the device-to-device variation. On the device side,

Gamma ray irradiation resulted in progressive resonant wavelength shifts with increasing radiation dose (Fig. 2b). The observed resonant wavelength shift was a combined effect of radiation-induced refractive index changes in the SiC core (Δn_{core}) and SiO₂ cladding (Δn_{clad}). To elucidate the respective contributions from the core and cladding, micro-ring resonators with different core widths (from 700 nm to 1000 nm) but otherwise identical configurations (275 nm core height, 150 μm diameter) were fabricated on the same chip. Waveguides with different dimensions give rise to varying confinement factors Γ_{core} and Γ_{clad} in the core and cladding regions, respectively. The measured resonant wavelength drift $\Delta\lambda$ relates to the modal effective index change caused by irradiation Δn_{eff} through:

$$\Delta\lambda = \frac{\Delta n_{\text{eff}}}{n_g} \cdot \lambda = \left(\Gamma_{\text{core}} \Delta n_{\text{core}} + \Gamma_{\text{clad}} \Delta n_{\text{clad}} \right) \cdot \frac{\lambda}{n_g} \quad (1)$$

Here λ denotes the starting resonant wavelength and n_g is the group index. It is important to note that Γ_{core} and Γ_{clad} in general do not add up to unity due to the slow light effect³⁴. We define normalized confinement factors as follows:

$$\Gamma_{\text{norm,core}} = \frac{\Gamma_{\text{core}}}{\Gamma_{\text{core}} + \Gamma_{\text{clad}}} \quad \text{and} \quad \Gamma_{\text{norm,clad}} = \frac{\Gamma_{\text{clad}}}{\Gamma_{\text{core}} + \Gamma_{\text{clad}}} \quad (2)$$

We see that the sum of so-defined $\Gamma_{\text{norm,core}}$ and $\Gamma_{\text{norm,clad}}$ always equals to unity. Eq. 1 can then be cast in the following form:

$$\frac{\Delta n_{\text{eff}}}{\Gamma_{\text{core}} + \Gamma_{\text{clad}}} = \Gamma_{\text{norm,core}} \Delta n_{\text{core}} + (1 - \Gamma_{\text{norm,core}}) \Delta n_{\text{clad}} = (\Delta n_{\text{core}} - \Delta n_{\text{clad}}) \Gamma_{\text{norm,core}} + \Delta n_{\text{clad}} \quad (3)$$

Eq. 3 suggests that the measured $\Delta n_{\text{eff}} / (\Gamma_{\text{core}} + \Gamma_{\text{clad}})$ for all the resonators and polarizations at a given radiation dose, when plotted as a function of $\Gamma_{\text{norm,core}}$, should fall on a straight line. As is seen in an example shown in Fig. 2c, this is indeed the case and linear fits of our measured data consistently give coefficients of determination (R^2) above 0.99. The intercepts of the fitted line with $\Gamma_{\text{norm,core}} = 1$ and $\Gamma_{\text{norm,core}} = 0$ then correspond to Δn_{core} and Δn_{clad} respectively with the particular radiation dose.

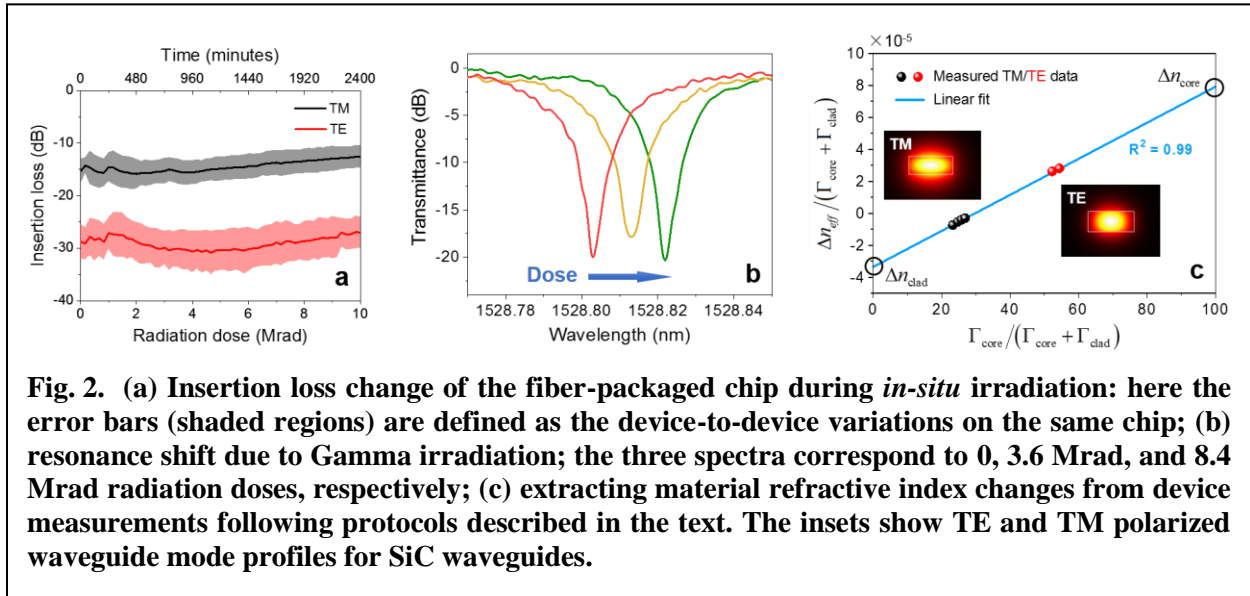
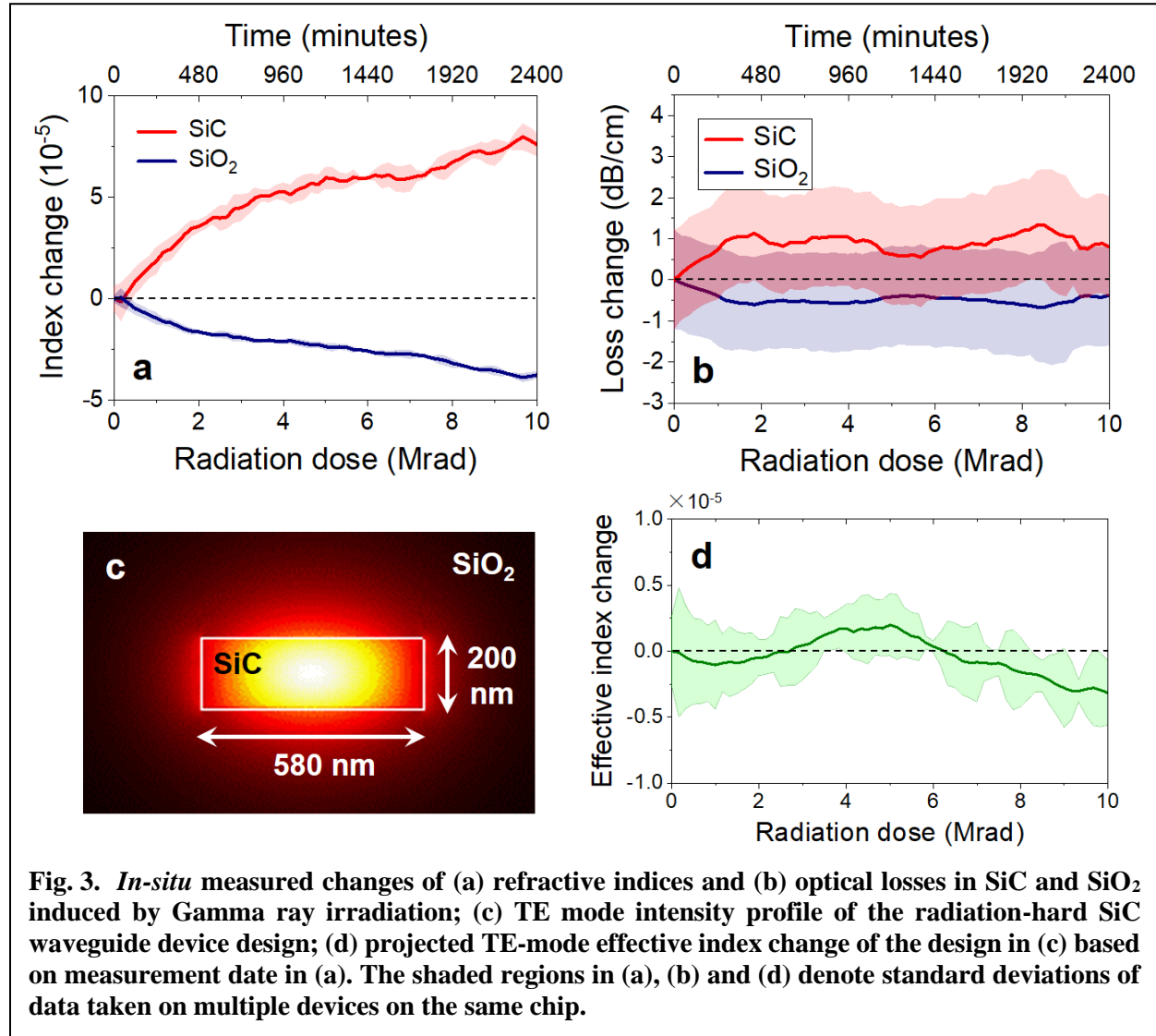


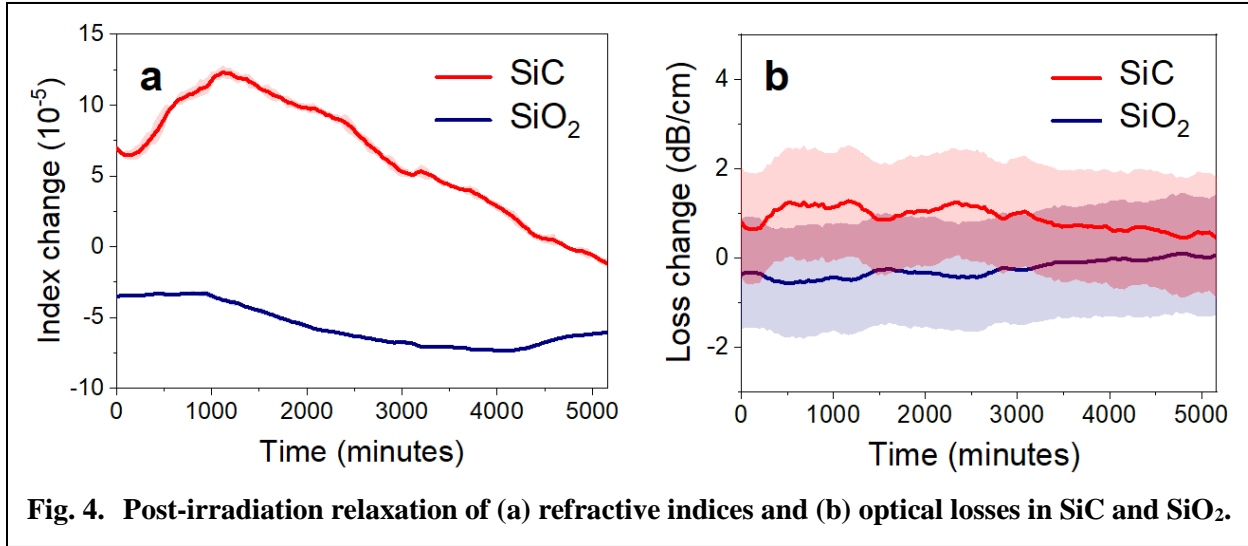
Fig. 2. (a) Insertion loss change of the fiber-packaged chip during *in-situ* irradiation: here the error bars (shaded regions) are defined as the device-to-device variations on the same chip; (b) resonance shift due to Gamma irradiation; the three spectra correspond to 0, 3.6 Mrad, and 8.4 Mrad radiation doses, respectively; (c) extracting material refractive index changes from device measurements following protocols described in the text. The insets show TE and TM polarized waveguide mode profiles for SiC waveguides.

Besides inferring the refractive index changes of core and cladding materials, the same notion can also be applied to extract the optical loss variations in both materials from the quality factor (Q-factor) modifications of the different resonator devices and polarizations. The detailed formalism of the loss extraction procedure is presented in the Supporting Information.



Figures 3a and 3b plot the radiation dose dependent changes in material refractive indices and optical losses, respectively. Optical losses in the materials hardly changed within the measurement error throughout the course of the irradiation experiment. The relatively large dispersion in the measured optical losses (approximately ± 1 dB/cm) is attributed to inherent scattering loss variations in micro-ring resonators³⁵. In contrast, refractive index changes ranging from 10^{-5} to 10^{-4} were unambiguously quantified taking advantage of the extreme precision afforded by resonant cavity refractometry³⁶⁻³⁸. This index drift is sufficiently small to be negligible for most guiding wave devices, however it must be properly compensated in devices sensitive to optical phase variations, such as MZIs and resonators. It is also interesting to note that SiC and SiO₂ exhibit index changes with opposing signs. This observation signals the possibility of creating radiation-hard optical devices by engineering the modal confinement to nullify the effective index drift. One

such hypothetical design is illustrated in Fig. 3c, and the projected dose-dependent effective index change of the device is plotted in Fig. 3d based on the measured index change values in Fig. 3a. The design predicts waveguide effective index drift of less than 2×10^{-6} , more than an order of magnitude smaller than the index changes of SiC or SiO₂ alone. Such a design is useful in improving phase stability of photonic components in radiation environments.



The packaged device also facilitates real-time tracking of the materials' post-radiation relaxation response at room temperature. Figures 4a and 4b plot the refractive index and loss relaxation behavior of SiC and SiO₂ after 10 Mrad Gamma irradiation. While the loss variation is insignificant, we observed considerable refractive index change in SiC. Remarkably, the post-radiation index change in SiC over time is not a monotonic function, showing an initial increase followed by subsequent decrease. This is in contrast to refractive index relaxation in crystalline Si, which occurs immediately after irradiation is terminated and always acts to diminish the index change induced by radiation¹⁵.

The results from our *in-situ* measurement outlined above provide important insights into the mechanism of radiation damage in a-SiC for photonic applications. In general, there are three possible damage mechanisms caused by Gamma radiation which can lead to optical property modifications: 1) ionizing radiations generate electron and hole pairs which introduce free carrier absorption and refractive index change through the plasmon dispersion effect³⁹; 2) high-energy photons or particles can catalyze oxidation reactions. For instance, Gamma radiation was reported to induce surface oxidation and refractive index change in SiN and a-Si when the samples were exposed to an ambient environment¹¹; and 3) while direct momentum transfer from the photons of Gamma rays to atoms is minimal, high-energy electrons emitted through the Compton scattering process can collide with atoms and produce point (displacement) defects⁴⁰. Formation of these point defects further triggers drastic rise in local temperature and pressure, which prompts local network configuration and density change in an amorphous material⁴¹.

Here we argue that volume compaction due to Compton scattering displacement is the main mechanism responsible for the observed optical property change in SiC. In a-SiC, the free carrier effects are negligible due to low carrier mobility. In addition, the persistent refractive index change after removal of the sample from irradiation chamber can hardly be accounted for by free carrier effects. Our SiC devices are entirely encapsulated in a SiO₂ cladding and isolated from the ambient

atmosphere. Moreover, we have performed secondary-ion mass spectrometry (SIMS) measurements on Gamma-irradiated a-SiC to confirm the absence of surface oxidation (see Supporting Information).

To further reinforce the argument, we computed of the atomic displacement parameters in SiC and the results are summarized in Table 1. Details of the calculations are furnished in the Supporting Information. The calculated maximum atomic recoil energies are significantly larger than the displacement energy threshold in a-SiC (13 eV⁴²), and thus the Compton scattered electrons have a high probability of causing displacement damage in the material. The total density of displacement defects is approximately 5.8×10^{14} /cm³, or 5.8×10^{-9} per atomic site. The heat and pressure spikes produced by each displacement defect can impact a large number of nearby atoms⁴¹ and remove excess free volume in as-deposited a-SiC through local bond rearrangement, thereby leading to the refractive index change.

Table 1. Calculated displacement damage parameters in a-SiC at 10 Mrad radiation dose

Atom type	Maximum recoil energy (eV)	Compton scattering displacement cross-section (barn, 10^{-22} cm ²)	Gamma photon fluence (/cm ²)	Atomic density (/cm ³)	Density of displacement defects (/cm ³)
Silicon (Si)	204	0.45	1.9×10^{16}	6.6×10^{22}	5.6×10^{14}
Carbon (C)	476	0.28	1.9×10^{16}	3.4×10^{22}	1.8×10^{14}

To account for the non-monotonic relaxation behavior, we note that unlike crystalline materials, the structure of amorphous compounds are characterized by a large number of metastable configurations or metabasins⁴³. Structural relaxation (or aging) in amorphous materials is therefore an inherently complex process and does not necessarily retraces back to the starting structural state⁴⁴. Moreover, since the a-SiC deposited by PECVD is heavily hydrogenated (see Supporting Information), the structural relaxation kinetics may be further complicated by hydrogen diffusion, which can contribute to generation or passivation of broken (dangling) bonds in a-SiC and stabilize metastable structural configurations after irradiation⁴⁵. Exact structural origin of the post-radiation relaxation behavior will be a topic worthy of further investigations.

In conclusion, in this study we developed a method to probe optical property changes of photonic materials induced by ionizing radiations through *in-situ* photonic device measurements. We show that the photonic package is stable in the Gamma radiation environment and permits long-term, real-time measurements up to a large radiation dose. The radiation-induced refractive index change in SiC is attributed to volume compaction resulting from displacement defects generated by Compton scattered electrons. We also observed a non-monotonic variation of the SiC material refractive index during room-temperature post-radiation relaxation. Finally, findings from the study further points to the potential of realizing radiation-hard passive photonic devices leveraging the opposite signs of radiation-induced refractive index changes in different materials.

Methods

Device fabrication. The devices were fabricated on piranha cleaned Si wafers. The process started with growing a 2- μ m-thick PECVD SiO₂ under cladding layer. A 275-nm film of amorphous silicon carbide was deposited subsequently via PECVD with a gas mixture of CH₄ and SiH₄ following previously published conditions²¹. Patterning of the SiC film was conducted on an Elionix ELS-F125 electron beam lithography (EBL) tool with a beam current of 10 nA and an optimized dose of 3200 μ C/cm². 6% hydrogen silsesquioxane (HSQ) was chosen as the EBL resist as it provides optimal etching resistivity. The chip was then developed in 25% tetramethylammonium hydroxide (TMAH) for 2.5 min to reveal the pattern. Reactive ion etching was performed in an STS ICP-RIE tool with a forward power of 1000 W and an etching gas of Cl₂

at a pressure of 30 mTorr. These parameters yielded an etching rate of a-SiC at 600 nm/min. Device fabrication was completed by depositing another 2 μm PECVD oxide layer as the top cladding. The devices fabricated following the protocols are symmetrically cladded with PECVD SiO₂. The cross-sectional dimensions of the waveguides were quantified using scanning electron microscopy (SEM) and used as input parameters for full-vectorial optical modal simulations.

Device packaging. The as-fabricated devices were packaged with optical fiber arrays (SQS Vlaknova optika a.s.) using UV curable epoxy (Masterbond UV15TK) as the bonding agent. Fibers with an incident angle of 15° were first active aligned to the on-chip grating couplers to maximize the transmitted power. Epoxy was applied onto the chip to securely bond the fibers to the chip. Active alignment was repeated after epoxy application to ensure optimal coupling. The epoxy was then cured through flood UV exposure. After the epoxy was fully cured, the fibers were released from the alignment stage and attached to a custom-designed and 3-D printed device holder.

Acknowledgement

The authors acknowledge funding support provided by Defense Threat Reduction Agency (DTRA) under HDTRA1-15-1-0060, and material characterization and fabrication facility support by the MIT Center of Materials Science & Engineering (CMSE) and the Microsystems Technology Laboratories (MTL).

References

1. Asghari, M.; Krishnamoorthy, A. V. Energy-Efficient Communication. *Nat. Photonics* **2011**, *5* (5), 268–270.
2. Marpaung, D.; Yao, J.; Capmany, J. Integrated Microwave Photonics. *Nat. Photonics* **2019**, *13* (2), 80–90.
3. Kita, D. M.; Miranda, B.; Favela, D.; Bono, D.; Michon, J.; Lin, H.; Gu, T.; Hu, J. High-Performance and Scalable on-Chip Digital Fourier Transform Spectroscopy. *Nat. Commun.* **2018**, *9* (1), 4405.
4. El Nasr-Storey, S. S.; Boeuf, F.; Baudot, C.; Detraz, S.; Fedeli, J.-M.; Marris-Morini, D.; Olantera, L.; Pezzullo, G.; Sigaud, C.; Soos, C.; et al. Silicon Photonics for High Energy Physics Data Transmission Applications. In *11th International Conference on Group IV Photonics (GFP)*; IEEE, 2014; pp 1–2.
5. Duarte, V. C.; Prata, J. G.; Nogueira, R. N.; Winzer, G.; Zimmermann, L.; Walker, R.; Clements, S.; Filipowicz, M.; Napierala, M.; Nasilowski, T.; et al. Modular and Smooth Introduction of Photonics in High-Throughput Communication Satellites – Perspective of Project BEACON. **2019**, *11180*, 1118079.
6. Ahmed, Z.; Cumberland, L. T.; Klimov, N. N.; Pazos, I. M.; Tosh, R. E.; Fitzgerald, R. Assessing Radiation Hardness of Silicon Photonic Sensors. *Sci. Rep.* **2018**, *8* (1), 13007.
7. Kraxner, A.; Detraz, S.; Olantera, L.; Scarcella, C.; Sigaud, C.; Soos, C.; Troska, J.; Vasey, F. Investigation of the Influence of Temperature and Annealing on the Radiation Hardness of Silicon Mach–Zehnder Modulators. *IEEE Trans. Nucl. Sci.* **2018**, *65* (8), 1624–1631.
8. Zeiler, M.; El Nasr-Storey, S. S.; Detraz, S.; Kraxner, A.; Olantera, L.; Scarcella, C.; Sigaud, C.; Soos, C.; Troska, J.; Vasey, F. Radiation Damage in Silicon Photonic Mach–Zehnder Modulators and Photodiodes. *IEEE Trans. Nucl. Sci.* **2017**, *64* (11), 2794–2801.
9. Arutt, C. N.; Alles, M. L.; Liao, W.; Gong, H.; Davidson, J. L.; Schrimpf, R. D.; Reed, R. A.; Weller, R. A.; Bolotin, K.; Nicholl, R.; et al. The Study of Radiation Effects in Emerging Micro and Nano Electro Mechanical Systems (M and NEMs). *Semicond. Sci. Technol.* **2017**, *32* (1), 013005.
10. Morichetti, F.; Grillanda, S.; Manandhar, S.; Shutthanandan, V.; Kimerling, L.; Melloni, A.; Agarwal, A. M. Alpha Radiation Effects on Silicon Oxynitride Waveguides. *ACS Photonics* **2016**, *3* (9), 1569–1574.
11. Du, Q.; Huang, Y.; Ogbuu, O.; Zhang, W.; Li, J.; Singh, V.; Agarwal, A. M.; Hu, J. Gamma Radiation Effects in Amorphous Silicon and Silicon Nitride Photonic Devices. *Opt. Lett.* **2017**, *42* (3), 587.
12. Brasch, V.; Chen, Q.-F.; Schiller, S.; Kippenberg, T. J. Radiation Hardness of High-Q Silicon Nitride Microresonators for Space Compatible Integrated Optics. *Opt. Express* **2014**, *22* (25), 30786.
13. Grillanda, S.; Singh, V.; Raghunathan, V.; Morichetti, F.; Melloni, A.; Kimerling, L.; Agarwal, A. M. Gamma Radiation Effects on Silicon Photonic Waveguides. *Opt. Lett.* **2016**, *41* (13), 3053.
14. Bhandaru, S.; Hu, S.; Fleetwood, D. M.; Weiss, S. M. Total Ionizing Dose Effects on Silicon Ring Resonators. *IEEE Trans. Nucl. Sci.* **2015**, *62* (1), 323–328.
15. Dumon, P.; Kappeler, R.; Barros, D.; McKenzie, I.; Doyle, D.; Baets, R. Measured Radiation Sensitivity of Silica-on-Silicon and Silicon-on-Insulator Micro-Photonic Devices for Potential Space Application. In *SPIE Proceedings*; Taylor, E. W., Ed.;

- International Society for Optics and Photonics, 2005; Vol. 5897, p 58970D.
16. Seif El Nasr-Storey, S.; Boeuf, F.; Baudot, C.; Detraz, S.; Fedeli, J. M.; Marris-Morini, D.; Olantera, L.; Pezzullo, G.; Sigaud, C.; Soos, C.; et al. Effect of Radiation on a Mach-Zehnder Interferometer Silicon Modulator for HL-LHC Data Transmission Applications. *IEEE Trans. Nucl. Sci.* **2015**, *62* (1), 329–335.
 17. Nasr-Storey, S. S. El; Détraz, S.; Olanterä, L.; Sigaud, C.; Soós, C.; Pezzullo, G.; Troska, J.; Vasey, F.; Zeiler, M. Neutron and X-Ray Irradiation of Silicon Based Mach-Zehnder Modulators. *J. Instrum.* **2015**, *10* (03), C03040–C03040.
 18. Weber, W. J.; Jiang, W.; Thevuthasan, S. Defect Annealing Kinetics in Irradiated 6H–SiC. *Nucl. Instruments Methods Phys. Res. Sect. B Beam Interact. with Mater. Atoms* **2000**, *166–167*, 410–414.
 19. Sellin, P. J.; Vaitkus, J. New Materials for Radiation Hard Semiconductor Detectors. *Nucl. Instruments Methods Phys. Res. Sect. A Accel. Spectrometers, Detect. Assoc. Equip.* **2006**, *557* (2), 479–489.
 20. Lu, X.; Lee, J. Y.; Rogers, S.; Lin, Q. Optical Kerr Nonlinearity in a High-Q Silicon Carbide Microresonator. *Opt. Express* **2014**, *22* (25), 30826.
 21. Xing, P.; Ma, D.; Ooi, K. J. A.; Choi, J. W.; Agarwal, A. M.; Tan, D. CMOS-Compatible PECVD Silicon Carbide Platform for Linear and Nonlinear Optics. *ACS Photonics* **2019**, *6* (5), 1162–1167.
 22. Song, B.-S.; Yamada, S.; Noda, S.; Asano, T. Demonstration of Two-Dimensional Photonic Crystals Based on Silicon Carbide. *Opt. Express, Vol. 19, Issue 12, pp. 11084–11089* **2011**, *19* (12), 11084–11089.
 23. Zheng, Y.; Pu, M.; Yi, A.; Chang, B.; You, T.; Huang, K.; Kamel, A. N.; Henriksen, M. R.; Jørgensen, A. A.; Ou, X.; et al. High-Quality Factor, High-Confinement Microring Resonators in 4H-Silicon Carbide-on-Insulator. *Opt. Express* **2019**, *27* (9), 13053.
 24. Fan, T.; Moradinejad, H.; Wu, X.; Eftekhar, A. A.; Adibi, A. High-Q Integrated Photonic Microresonators on 3C-SiC-on-Insulator (SiCOI) Platform. *Opt. Express* **2018**, *26* (20), 25814.
 25. Magyar, A. P.; Bracher, D.; Lee, J. C.; Aharonovich, I.; Hu, E. L. High Quality SiC Microdisk Resonators Fabricated from Monolithic Epilayer Wafers. *Appl. Phys. Lett.* **2014**, *104* (5), 051109.
 26. Cardenas, J.; Zhang, M.; Phare, C. T.; Shah, S. Y.; Poitras, C. B.; Guha, B.; Lipson, M. High Q SiC Microresonators. *Opt. Express* **2013**, *21* (14), 16882.
 27. Chatzopoulos, I.; Martini, F.; Cernansky, R.; Politi, A. High-Q/V Photonic Crystal Cavities and QED Analysis in 3C-SiC. *ACS Photonics* **2019**, acsphotonics.8b01671.
 28. Allieux, D.; Belarouci, A.; Hudson, D.; Magi, E.; Sinobad, M.; Beaudin, G.; Michon, A.; Singh, N.; Orobtschouk, R.; Grillet, C. Toward Mid-Infrared Nonlinear Optics Applications of Silicon Carbide Microdisks Engineered by Lateral under-Etching [Invited]. *Photonics Res.* **2018**, *6* (5), B74.
 29. Radulaski, M.; Babinec, T. M.; Buckley, S.; Rundquist, A.; Provine, J.; Alassaad, K.; Ferro, G.; Vučković, J. Photonic Crystal Cavities in Cubic (3C) Polytype Silicon Carbide Films. *Opt. Express* **2013**, *21* (26), 32623.
 30. Calusine, G.; Politi, A.; Awschalom, D. D. Silicon Carbide Photonic Crystal Cavities with Integrated Color Centers. *Appl. Phys. Lett.* **2014**, *105* (1), 011123.
 31. Lohrmann, A.; Karle, T. J.; Sewani, V. K.; Laucht, A.; Bosi, M.; Negri, M.; Castelletto, S.; Prawer, S.; McCallum, J. C.; Johnson, B. C. Integration of Single-Photon Emitters into

- 3C-SiC Microdisk Resonators. *ACS Photonics* **2017**, *4* (3), 462–468.
32. Bracher, D. O.; Hu, E. L. Fabrication of High- Q Nanobeam Photonic Crystals in Epitaxially Grown 4H-SiC. *Nano Lett.* **2015**, *15* (9), 6202–6207.
 33. Lu, X.; Lee, J. Y.; Feng, P. X.-L.; Lin, Q. High Q Silicon Carbide Microdisk Resonator. *Appl. Phys. Lett.* **2014**, *104* (18), 181103.
 34. Robinson, J. T.; Preston, K.; Painter, O.; Lipson, M. First-Principle Derivation of Gain in High-Index-Contrast Waveguides. *Opt. Express* **2008**, *16* (21), 16659.
 35. Li, Q.; Eftekhar, A. A.; Xia, Z.; Adibi, A. Azimuthal-Order Variations of Surface-Roughness-Induced Mode Splitting and Scattering Loss in High- Q Microdisk Resonators. *Opt. Lett.* **2012**, *37* (9), 1586.
 36. Hu, J.; Sun, X.; Agarwal, A.; Kimerling, L. C. Design Guidelines for Optical Resonator Biochemical Sensors. *J. Opt. Soc. Am. B* **2009**, *26* (5), 1032.
 37. Hu, J.; Torregiani, M.; Morichetti, F.; Carlie, N.; Agarwal, A.; Richardson, K.; Kimerling, L. C.; Melloni, A. Resonant Cavity-Enhanced Photosensitivity in As₂S₃ Chalcogenide Glass at 1550 Nm Telecommunication Wavelength. *Opt. Lett.* **2010**, *35* (6), 874.
 38. Hu, J.; Carlie, N.; Feng, N.-N.; Petit, L.; Agarwal, A.; Richardson, K.; Kimerling, L. Planar Waveguide-Coupled, High-Index-Contrast, High- Q Resonators in Chalcogenide Glass for Sensing. *Opt. Lett.* **2008**, *33* (21), 2500.
 39. De Leonardis, F.; Troia, B.; Campanella, C. E.; Prudeniano, F.; Passaro, V. M. N. Modeling of Radiation Effects in Silicon Photonic Devices. *IEEE Trans. Nucl. Sci.* **2015**, *62* (5), 2155–2168.
 40. Kwon, J.; Motta, A. T. Gamma Displacement Cross-Sections in Various Materials. *Ann. Nucl. Energy* **2000**, *27* (18), 1627–1642.
 41. Piao, F.; Oldham, W. G.; Haller, E. E. The Mechanism of Radiation-Induced Compaction in Vitreous Silica. *J. Non. Cryst. Solids* **2000**, *276* (1–3), 61–71.
 42. Cowen, B. J.; El-Genk, M. S. Point Defects Production and Energy Thresholds for Displacements in Crystalline and Amorphous SiC. *Comput. Mater. Sci.* **2018**, *151*, 73–83.
 43. Ediger, M. D.; Harrowell, P. Perspective: Supercooled Liquids and Glasses. *J. Chem. Phys.* **2012**, *137* (8), 080901.
 44. Geiger, S.; Du, Q.; Huang, B.; Shalaginov, M. Y.; Michon, J.; Lin, H.; Gu, T.; Yadav, A.; Richardson, K. A.; Jia, X.; et al. Understanding Aging in Chalcogenide Glass Thin Films Using Precision Resonant Cavity Refractometry. *Opt. Mater. Express* **2019**, *9* (5), 2252.
 45. Imagawa, O.; Yasuda, K.; Yoshida, A. Gamma-ray Irradiation Effect in Amorphous Hydrogenated Silicon. *J. Appl. Phys.* **1989**, *66* (10), 4719–4722.